Initial stages of corrosion within Mg-Zn-Y-Zr alloy in 1 g/l NaCl solution

I. POPOV, D. STAROSVETSKY, D. SHECHTMAN
Department of Materials Engineering, TECHNION–Israel Institute of Technology, Technion City, Haifa 32000, Israel
E-mail: mtrdan@vmsa.technion.as.il

Corrosion behavior of as-cast and heat treated Mg-Zn-Zr-Y alloy was studied in 1 g/l NaCl solution. The as-cast alloy was the least resistant to pitting corrosion. Its Mg-Zn solid solution matrix was the structural constituent responsible for corrosion susceptibility due to the presence of Zn-lean regions. Homogenization of the Zn distribution within the matrix significantly increased the corrosion resistance of the alloy. Grain boundaries, which contain intermetallic phases, were resistant to corrosion attack, thus impeding corrosion propagation.

1. Introduction

Among magnesium-based alloys, the group of Mg-RE alloys is known to have the best high temperature mechanical properties [1, 2]. These alloys also demonstrate better corrosion resistance than Mg-Al-Zn and Mg-Al-Mn alloys [3, 4]. It has recently been shown [5] that addition of Zn to Mg-RE-Zr alloys coupled with reduction in RE content enhances the mechanical properties over a large temperature range. It has also been found that these alloys contain several Zn-enriched intermetallics including a thermodynamically stable quasicrystalline ternary phase $Mg_{30}Zn_{60}Y_{10}$ [6–8]. Addition of Zn is usually considered as harmful to corrosion resistance of magnesium alloys [9]. However, the corrosion behavior of Mg-RE-Zr alloys containing Zn has not yet been studied. The purpose of the present study was to evaluate the corrosion behavior of Mg-Zn-Y-Zr alloy and to determine the structural constituent, which has the lowest corrosion resistance.

2. Experimental techniques

The Mg-Zn-Y-Zr alloy contained 1.96 at % Zn, 0.16 at % Y, 0.11 at % Zr, balance Mg. The alloy was melted in an electrical furnace at 720 °C and cast into an air-cooled metal mould. The chemical composition of the as-prepared alloy was determined by quantum spectroscopy using a BAIRD DV/5 spark emission spectrometer.

Corrosion behavior was studied for two conditions of the alloy: (1) 100 h at 220 °C and (2) 1.5 h at 500 °C. All specimens were heat treated within sealed quartz tubes, which had a vacuum of 10^{-4} Torr. The heat treatment was performed in a preheated furnace and was terminated by rapid cooling in water.

Electrochemical tests used pencil-type electrodes 3 mm in diameter mounted in an epoxy resin. The electrodes were freshly abraded to 1000 grit prior to the corrosion test. The corrosion and electrochemical behavior of the alloy was studied in 1 g/l NaCl solution made from analytically pure reagent and double-distilled water. Tests were conducted in a 0.5 l conventional electrochemical cell at room temperature (22 ± 1 °C). Potentials were measured using Luggin capillar. The resulting potential values were referred to a saturated calomel electrode (SCE).

The regions, which underwent a localized corrosion attack, were examined to identify the micro-structural constituent responsible for pit initiation. In an effort to determine the relative position of corroded zones and structural constituents of alloy, the attacked surface was cleaned from the deposited corrosion products with Nital solution [10].

Microstructural observations were conducted by optical and scanning electron microscopy. The chemical composition of the different phases was determined by energy-dispersive X-ray spectroscopy (EDS).

3. Results

3.1. Microstructure

The microstructure of the as-cast alloy is shown in Fig. 1a. The matrix, which occupies 90% of the volume, was an inhomogeneous solid solution of Zn in Mg. It was formed by primary solidification of magnesium dendrites (Zn, Y and Zr in solid solution) below 620 °C. Most of the Y remained in the liquid, because the presence of Zn strongly decreases the Y solubility in solid magnesium. Solidification of the residual liquid formed several grain boundary eutectic (GBE) compositions. The phases found in the GBE are $Mg_{30}Zn_{60}Y_{10}$ ternary quasiperiodic phase, MgZn, Mg_7Zn_3 and magnesium-zinc solid solution. The presence of the thermodynamically unstable at room temperature Mg_7Zn_3 indicated that non-equilibrium solidification took place. This rapid solidification process resulted in inhomogeneity in the Zn distribution within the magnesium matrix. Fig. 1d shows that a single matrix grain consisted of

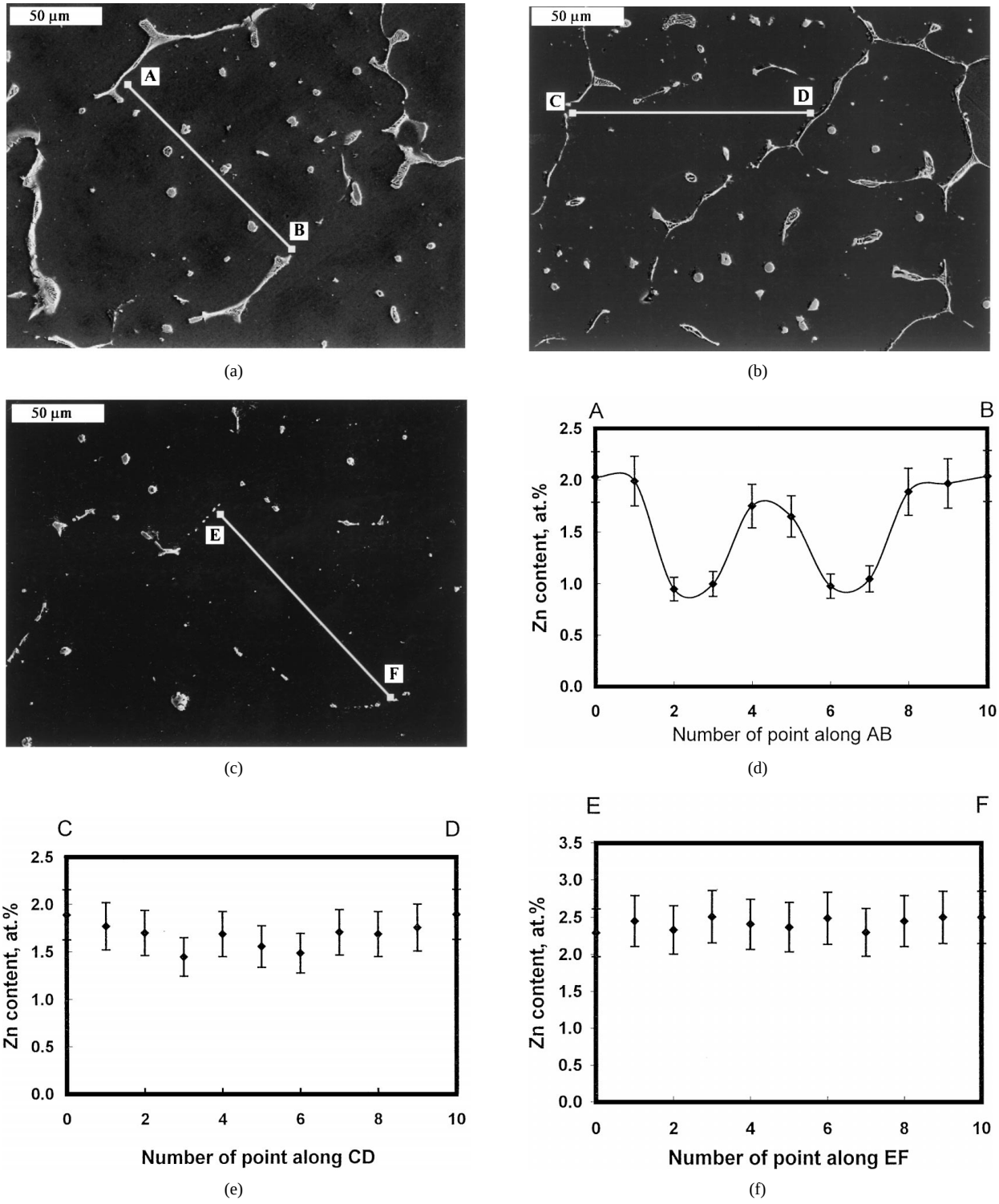

Figure 1 Microstructure of Mg-Zn-Y-Zr alloy: (a) as-cast, (b) after 100 h at 220 °C, (c) after 1.5 h at 500 °C. The graphs (d)–(f) present the Zn distribution along the lines AB, CD, EF, respectively.

Zn-poor (0.9–1.1 at % of Zn) as well as Zn-rich (1.8–2.0 at % of Zn) regions. The microstructure of the sample heat treated at 220 °C (see Fig. 1b) showed no visible differences from the as-cast alloy: the solid solution matrix and GBE were present in the same volume ratio (9 : 1) and had the same compositions. However, the Zn distribution within matrix grains (see Fig. 1e) was more homogeneous. The Zn concentration in a matrix grain was 1.4–1.7 at %.

Fig. 1c depicts the microstructure of the specimen heat treated at 500 °C for 1.5 h. This heat treatment has resulted in a significant decrease of GBE volume fraction (from 10 to 2%). Simultaneously, the solid solution matrix was enriched by Zn (up to 2.3–2.5 at %)—see Fig. 1f.

3.2. Electrochemical tests

Fig. 2 shows the corrosion potential (E_{corr}) transients for as-cast (curve 1) and heat-treated samples (curve 2–220 °C, 100 h; curve 3–550 °C, 1.5 h) in the NaCl solution. Initially, the values of E_{corr} for all three

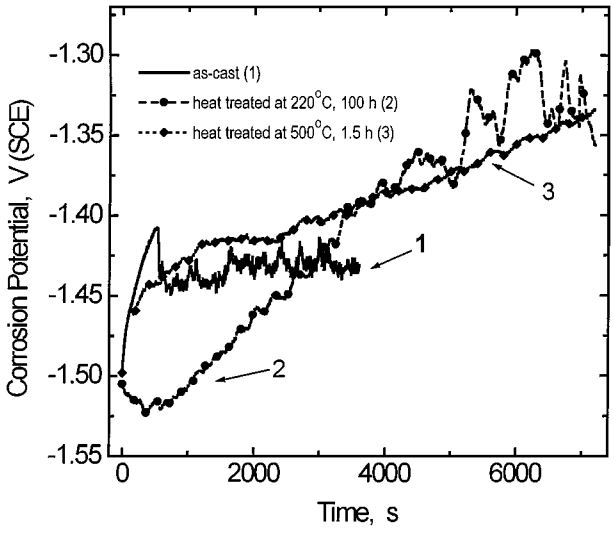

Figure 2 The corrosion potential transient of the specimens: 1—as-cast (solid line), 2—heat treated at 220 °C (dashed line, solid circles) and 3—heat treated at 500 °C (dashed line, solid diamonds).

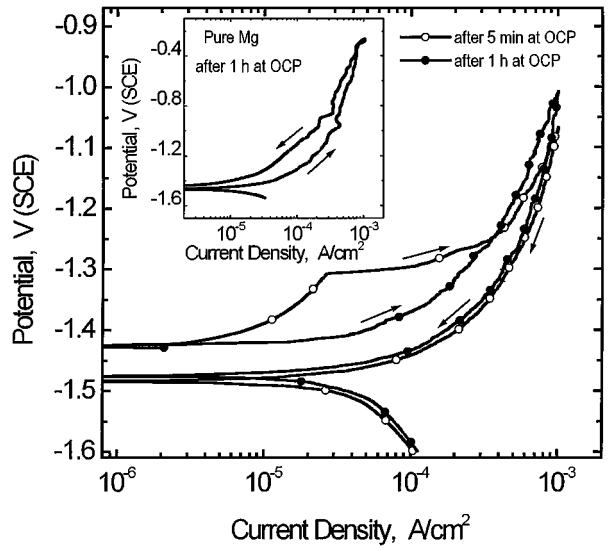

Figure 3 Cycling polarization curves for the as-cast alloy (scan rate of 1 mV/s): open circles—5-min pre-exposure at OCP; solid circles—1-hour pre-exposure at OCP. (Inset—polarization curve of pure Mg pre-exposed for 1 h at OCP recorded at the same scan rate).

electrodes were similar, about −1.5 V. The corrosion potential of the as-cast sample quickly shifted towards a more positive value, indicating surface film formation or passivation. Then, at −1.4 V, E_{corr} sharply decreased to −1.45 V, due to local surface activation, and remained at this value during the following after-breakdown exposure. The corrosion potential of the specimen heat-treated at 220 °C (see curve 2, Fig. 2) slightly decreased, and reached the lowest value of −1.52 V after exposure of 500 s. Then E_{corr} increased continually up to the stable value of −1.28 V. The corrosion potential of the specimen heat treated at 500 °C (curve 3, Fig. 2) gradually increased showing no evidence of breakdown during the entire test duration.

Fig. 3 presents the anodic curves obtained by cyclic polarization of the as-cast specimen exposed at OCP (open circle potential) for 5 min (curve 1, before breakdown) and 1 h (curve 2, after breakdown). The application of the polarization sweep after exposure of 5 min (curve 1) revealed that during the positive scan the electrode was passive up to −1.30 V where pitting initiated. Because cycling polarization measurements are used to determine both the potential of pitting corrosion (upon the positive scan) and the repassivation potential (upon the back scan) [11], the repassivation potential was measured on the back scan part of the curve at approx. −1.48 V. This corresponds to the stage at which active pitting sites were already repassivated and cathodic current value was relatively low. Upon the positive scan, no passivity region was observed on the sample broken down by 1 h exposure at OCP. A

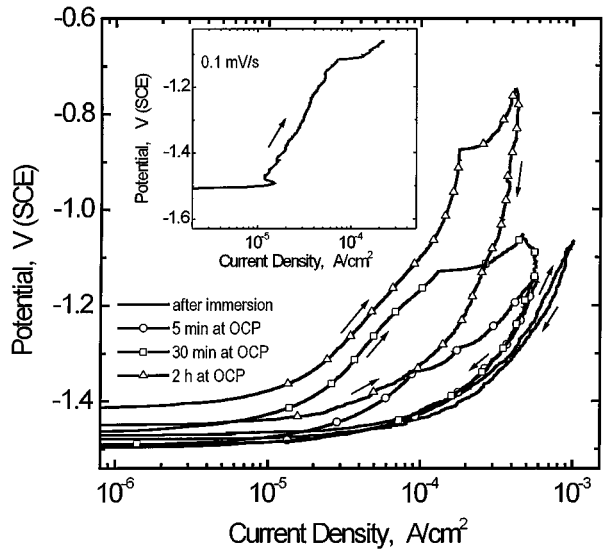

Figure 4 Cycling polarization curves of the specimen heat treated at 220 °C (scan rate of 1 mV/s): solid line without symbols—as-immersed specimen; open circles—5-min pre-exposure at OCP; open squares—30 min pre-exposure at OCP; open triangles—2-hours pre-exposure at OCP. (Inset—-anodic polarization of as-immersed specimen recorded at scan rate of 0.1 mV/s).

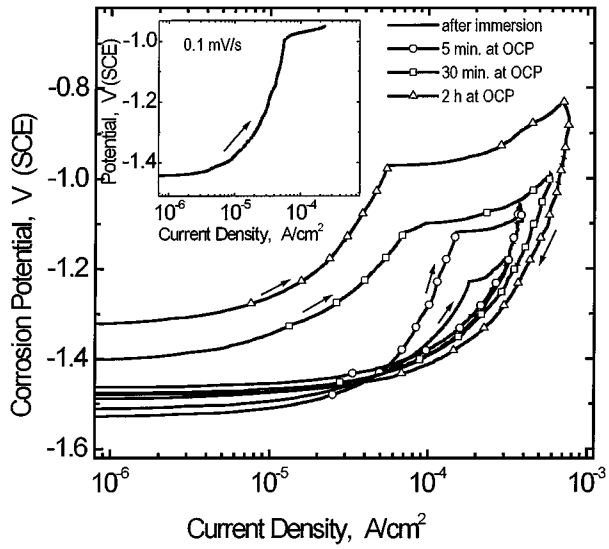

Figure 5 Cycling polarization curves for the sample heat treated at 500 °C (scan rate of 1 mV/s): solid line without symbols—as-immersed specimen; open circles—5-min pre-exposure at OCP; open squares—30-min pre-exposure at OCP; open triangles—2-hours pre-exposure at OCP. (Inset—anodic polarization of as-immersed specimen recorded at scan rate of 0.1 mV/s).

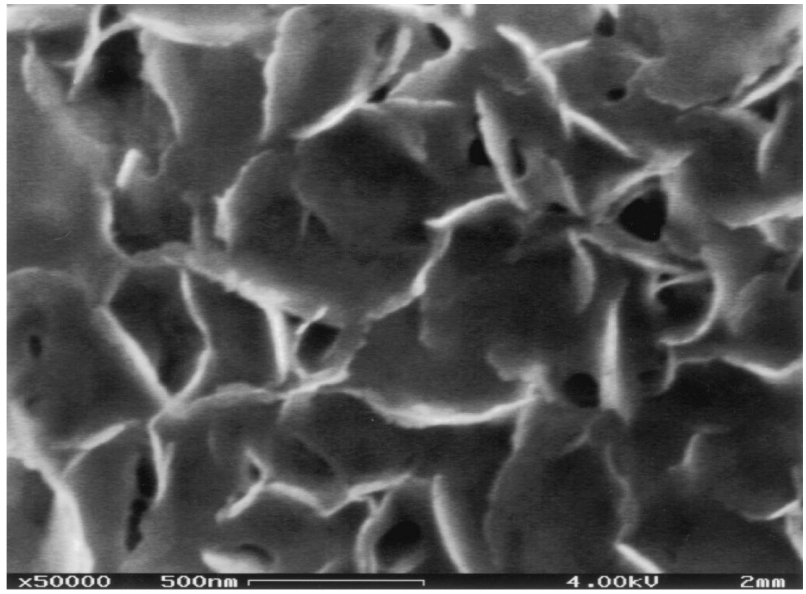

(a)

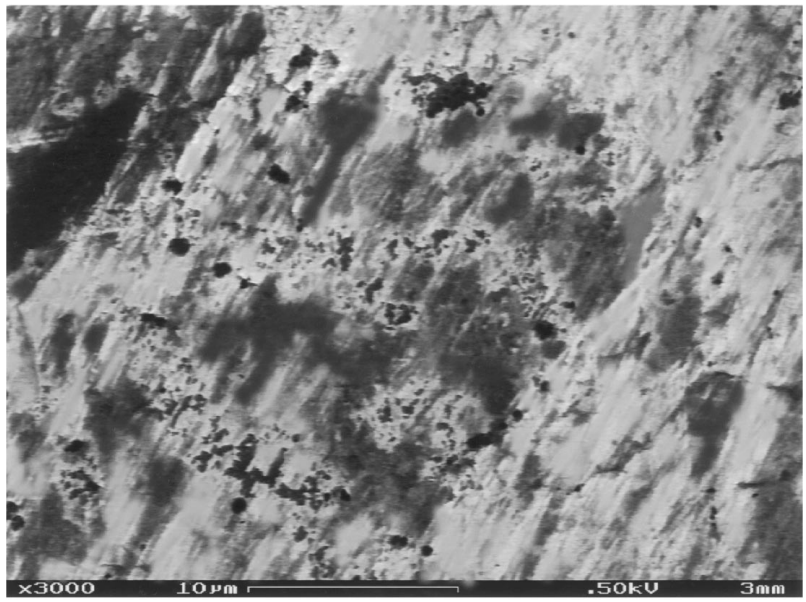

(b)

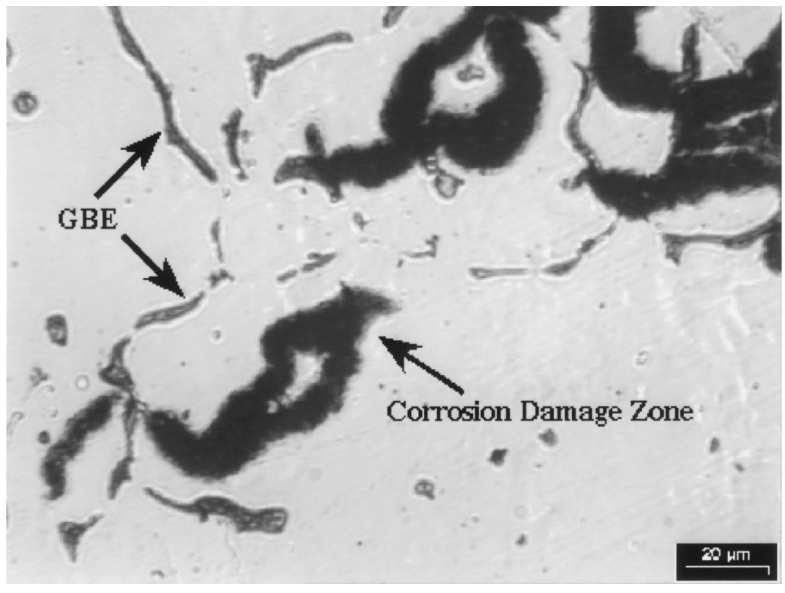

(c)

Figure 6 Microstructure of corroded as-cast alloy: (a) morphology of surface corrosion products layer; (b) pit initiation; (c) propagation of corroded zone ((a), (b)—SEM, (c)—optical microscopy).

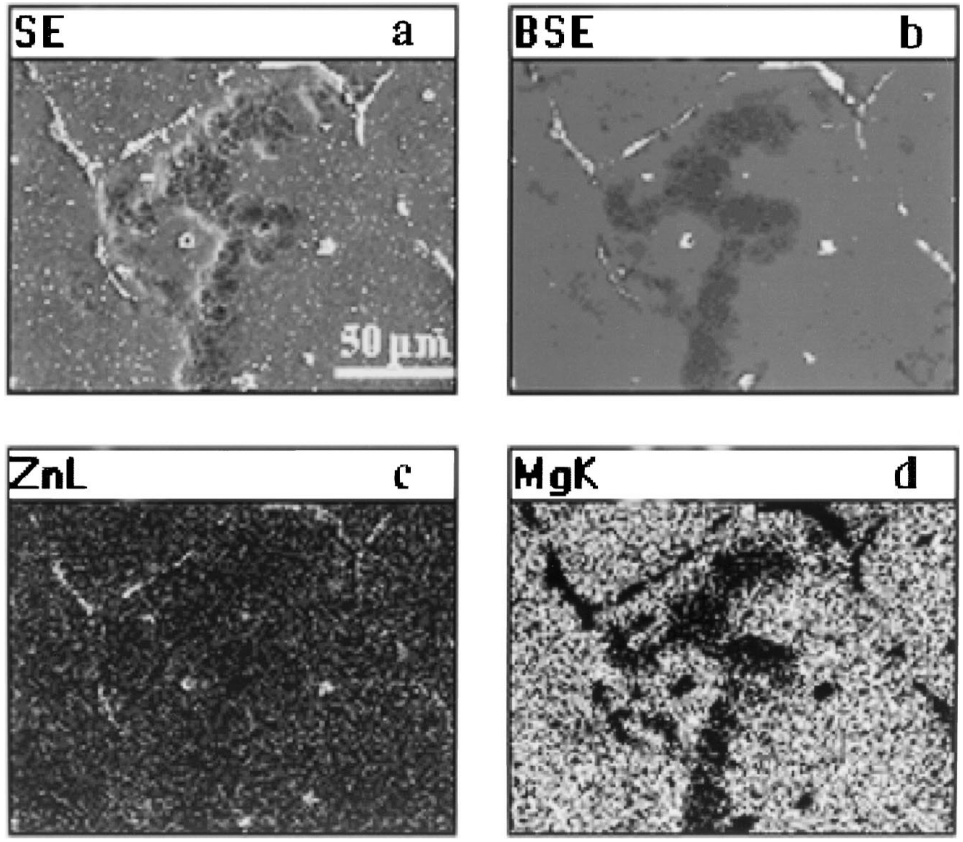

Figure 7 Distribution of Mg and Zn on the surface of corroded as-cast alloy: (a)–(d) are the images obtained with secondary electrons (SE), backscattered electrons (BSE), and Zn_L and Mg K_α X-ray radiation, respectively (EDS–SEM).

narrow loop between the positive and backscan parts of the curve was still observed, and was attributed to increasing the active area during the positive scan. The inset on Fig. 3 presents anodic curve of a pure magnesium specimen pre-exposed at OCP for 1 h. In contrast with the alloy, the pure magnesium was active over all the potential range. During the positive scan, its active surface was covered by corrosion products that decreased the anodic current on the backscan part of the curve.

Fig. 4 shows the anodic curves measured by cyclic polarization of the 220 °C heat-treated specimens following various exposure times at OCP. Positive and backscan parts of the anodic curve obtained immediately after immersion (with no pre-exposure, curve 1) practically coincide, indicating that the electrode was active and no protective layer was formed on its surface. Pre-exposure for 5 min at OCP (curve 2) was accompanied by some surface passivation appearing at the positive scan in narrow region of potentials—from −1.45 to −1.35 V when the breakdown occurred. It seems reasonable that such surface passivation was caused by a formation of protective layer, which contained the corrosion products. The breakdown was detected at −1.35 V while the repassivation of activated sites occurred at approx. −1.5 V.

Much stronger passivation was observed in specimens subjected to longer pre-exposures at OCP. A significant decrease of the anodic current in the potential region of passivity was measured. There was an increase in the breakdown potential of the sample pre-exposed for 30 min (curve 3) and the 2 h pre-exposed sample showed yet lower anodic current and nobler breakdown potential (curve 4). The values of the breakdown potential were −1.12 and −0.88 V for 30 min and 2 h pre-exposed specimens, respectively. In spite of the difference in breakdown potential, the repassivation of the active surface was detected also at the same potential of −1.5 V. Thus, the material annealed at 220 °C showed transition from the initial active state immediately upon immersion to the passive state becoming stronger with increasing exposure time at the OCP.

The transition from the active to the passive state can be clearly seen in potentiodynamic curves, obtained at the low scan rate, immediately after specimen immersion (inset, Fig. 4). An experiment conducted at a lower scan rate, revealed the presence of a small peak corresponding to the active-passive transition at −1.48 V.

The effect of pre-exposure at OCP on the anodic curves obtained by cyclic polarization of the 500 °C heat treated specimen is presented in Fig. 5. Compared with the former case, a faster passivation was observed in higher temperature heat treated material. A narrow passivity region (from −1.4 to −1.22 V) was detected even for the as-immersed specimen (curve 1). Increasing the pre-exposure time at OCP caused decrease in the anodic current in the passivity region followed by a simultaneous increase of the breakdown potential. For example, increasing the OCP pre-exposure from 5 min to 2 h (curves 2–4) resulted in a breakdown potential increase from −1.22 to −0.8 V. Thus, this microstructure enabled a faster formation of the protective layer, resulting in a lower anodic current values within a wide range of potentials. Such rapid passivation caused the

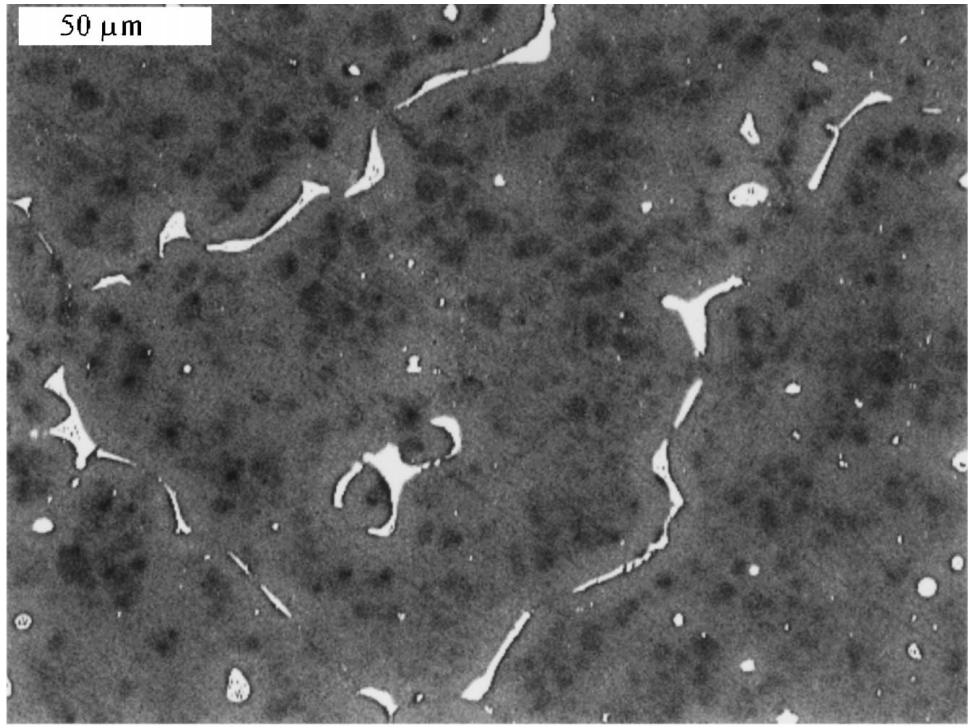

(a)

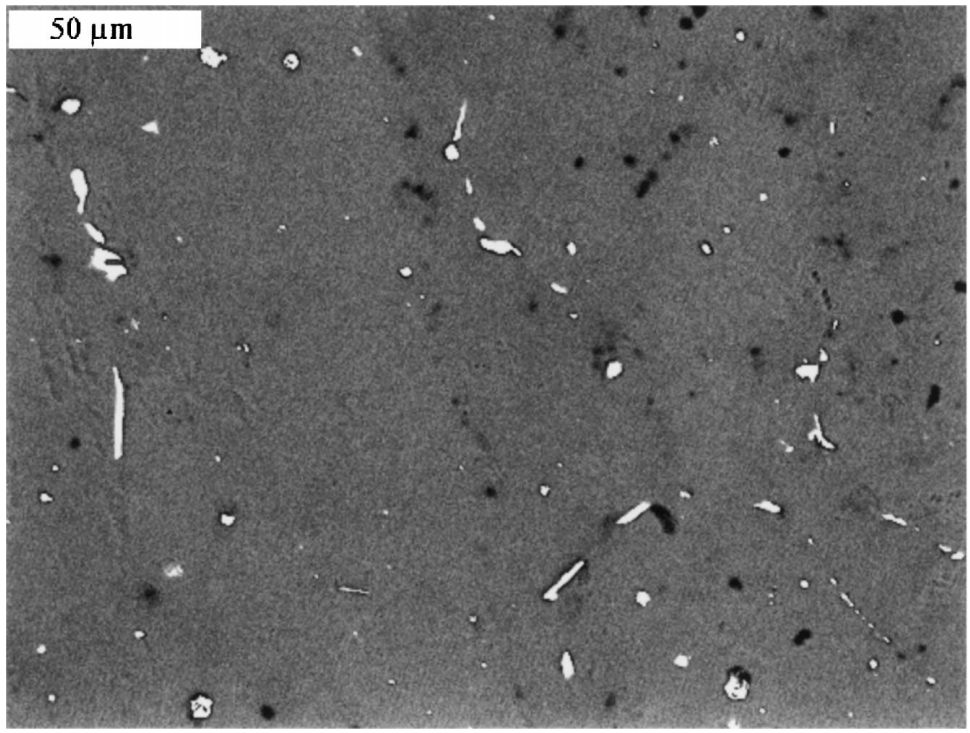

(b)

Figure 8 The attacked surface of specimen heat treated at 220 °C (a) and 500 °C (b) (SEM).

absence of active-to-passive transition on the positive scan obtained at lower scan rate (inset, Fig. 5).

3.3. The microstructure of the corroding material

Microstructural observation revealed an immediate formation of a corrosion product layer on the immersed surface of the tested specimens. Electron diffraction by TEM identified these layers as the oxide and hydroxide of magnesium. The morphology of such layer, created on the surface of as-cast alloy after immersion for 5 min at OCP (before breakdown) is shown in Fig. 6a, which presents the external surface of the as-cast specimen corroded in 1 g/l NaCl solution during 1 h. Fig. 6b shows the surface of the as-cast specimen after its exposure at OCP for 10 min (after breakdown, see solid curve 1 on Fig. 2). Immediately after breakdown, numerous small pits formed on the matrix grains of the as-cast alloy (Fig. 6b). All the initial pits were situated in Zn-lean regions, as seen from the HR SEM micrograph. A comparison between Fig. 1a (showing

distribution of Zn within the matrix grain) and Fig. 6b indicates that initially pits appeared on surfaces with Zn content less than 1.1 at %. In addition, as can be seen in Fig. 6c, during the following exposure, the corrosion front propagates also through the Zn-poor zone along the immersed surface. A corresponding map of Zn and Mg distribution within the corroded surface, presented on Fig. 7, indicated that the corrosion advances by a selective dissolution of magnesium. Thus, the zone of corrosion attack expanded along the sample surface as continuous shallow tracks.

Since no breakdown was detected in both heat-treated structures exposed at OCP, these materials were activated under polarization: a positive polarization sweep was applied to specimens pre-exposed for 30 min at OCP until the breakdown occurred. In both cases, initial pits appeared within the solid solution matrix (Fig. 8a and b). However, in the specimen subjected to low temperature annealing, numerous uniformly distributed pits were observed, while the sample, which was heat treated at a higher temperature showed only a small number of irregularly spaced pits.

3.4. Effect of short time cathodic treatment

The as-cast specimens underwent a local activation in 1g/l NaCl solution even after a short exposure at OCP. The corrosion attack was accompanied by a sharp decrease in the corrosion potential and in the number of active sites on the attacked surface. Short time exposure of activated specimens at potential less than −1.5 V (cathodic treatment), not only repassivated the active sites, but also strongly increases their passivity. Specimen passivity observed on the anodic curve obtained after 5 min exposure at −1.6 V, was characterized by a lower anodic current and much higher breakdown potential than that of the as-cast specimen (compare Fig. 9, curve 1 with Fig. 2, curve 1). Application of the same cathodic treatment to the heat treated specimens, which broke down potentiodymanically after 30 min pre-exposure at OCP, revealed a more pronounced increase in specimen passivity. As seen in Fig. 9 (curves 2 and 3), both heat treated specimens were passive after the cathodic treatment up to −0.5 V. Thus, they reached a much nobler value of breakdown potential than those produced by long OCP pre-exposure (Figs 3 and 4, curves 4). Additionally, broad hysteresis loops were observed for the specimens when cathodic treatment was applied.

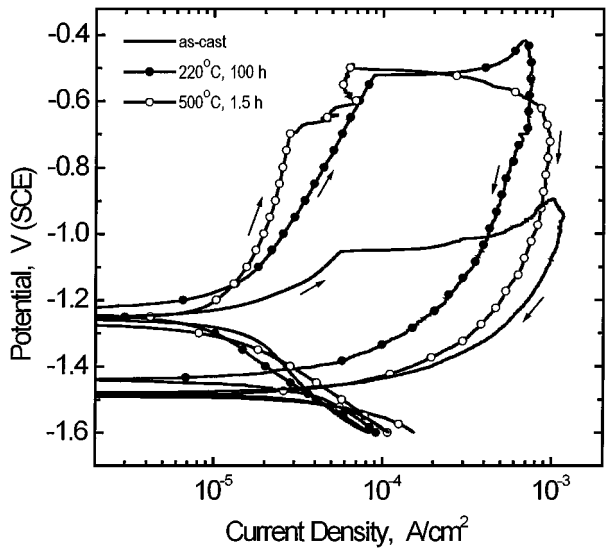

Figure 9 Cycling polarization curves of activated samples exposed for 5 min at −1.6 V: solid line without symbols present as-cast specimen; solid circles—heat treated at 220 °C, open circles—heat treated at 500 °C. Scan rate—1 mV/s.

4. Discussion

The tested alloy had a multiphase structure in both the as-cast and the heat-treated states. Grain boundaries, which contained intermetallics and were enriched by Zn and Y, were much less susceptible to corrosion attack than the solid solution matrix where all of the corrosion events occurred.

The corrosion behavior of the as-cast alloy indicated its solid solution matrix as a structural constituent that preferentially undergoes the corrosion attack. In the as-cast alloy, the matrix, which consists of Zn-lean (0.9–1.1 at %) and Zn-rich (1.9–2.0 at %) regions, underwent preferred activation at Zn-lean sites. Homogenization of the Zn distribution by low temperature annealing narrowed the limits of the Zn content variation to 1.4–1.7 at % compared to 0.9–2.0 at % in the as-cast material. In this case, the passivation took place slower than in the as-cast specimen. Immediately after immersion, the specimen was practically active and only after a 5 min exposure, a narrow passive region appeared on its anodic polarization curve. High temperature heat treatment significantly equilibrated and increased the Zn content (up to 2.3–2.5 at %) in the matrix. This increase markedly accelerated the subsequent passivation, which appeared on the anodic curve of as-immersed specimen and corresponded to a low value of anodic current.

Thus, increasing the Zn content in the matrix by a small percentage enhanced the corrosion resistance of the alloy. Our experiments show that the corrosion products, which formed on the immersed surface, provided corrosion resistance, as is the case in other magnesium alloys [12–15]. Although the corrosion products were identified as mainly magnesium oxide and hydroxide, the presence of zinc-based corrosion products should not be excluded. It is well known that corrosion properties of pure Zn in neutral water are determined by its corrosion products [16]. Therefore, it is reasonable to assume that Zn corrosion products contribute to the corrosion protection of our alloy.

Following the homogenization of the as-cast alloy, the protective properties of the corrosion products, which formed on its surface, were still not homogeneous. Obviously, the creation of a protective layer on the Zn-lean regions occurred slower than on those enriched by Zn. Consequently, the immersed surface consisted of specific matrix regions, which was anodic relative to the other structural constituents. Non-uniform formation of protective layers, as well as a fast positive shift of corrosion potential observed for these specimens after immersion, may cause the localization of

corrosion attack on the Zn-lean regions at relatively low values of corrosion potential. Zn-lean region activation, which was, in fact, dissolution of magnesium, resulted in the relative increase of Zn content in the remaining material. Therefore, the cathodic exposure at negative potential (in our case −1.6 V) may cause intensive repassivation of activated sites and the formation of a more uniform surface protective layer.

5. Summary

An electrochemical and microstructural study of corrosion behavior of Mg-Zn-Y-Zr alloy was performed in chloride containing water. The magnesium-zinc matrix of the alloy was found to be the most susceptible to localized corrosion attack with Zn-lean regions having the least corrosion resistance. The immediate formation of a corrosion product layer on the immersed surface provided the corrosion protection of the alloy. The protective properties of this layer were found to be dependent on Zn content and distribution within the matrix. The homogenization of zinc distribution and raising its content in the matrix by heat-treatment increases the corrosion resistance.

Acknowledgements

We wish to thank the Israel Consortium for the Development of Magnesium Technologies (Israel Ministry of Industry and Trade) and The Center for Absorption in Science (Israel Ministry of Immigrant Absorption) for their financial support. We gratefully acknowledge the use of the equipment in the Wolfson Center for Interface Science at the Technion.

References

1. I. J. POLMEAR, "Light Alloys" (Arnold, London, 1995) p. 200.
2. M. E. DRITZ, L. L. ROKHLIN, E. M. PADEZHNOVA *et al.*, "Magnesium Alloys Containing Yttrium" (Nauka, Moscow, 1979) p. 163.
3. P. L. MILLER, B. A. SHAW, R. G. WENDT *et al.*, *Corrosion* **49** (1993) 947.
4. W. UNSWORTH and J. KING, *Metallurgia* **53** (1986) 199.
5. Z. P. LUO, D. Y. SONG and S. Q. ZHANG, *Journal of Alloys and Compounds* **230** (1995) 109.
6. E. M. PADEZHNOVA, E. V. MEL'NIK and R. A. MILIEVSKIY *et al., Russian Metallurgy* **4** (1982) 185.
7. E. M. PADEZHNOVA, E. V. MEL'NIK and T. B. DOBATKINA, *Izvestia Akademii Nauk SSSR. Metalli* **1** (1979) 217.
8. Z. LUO and S. ZHANG, *J. Mater. Sci. Lett.* **12** (1993) 1490.
9. I. NAKATSUGAWA, S. KAMADO, Y. KOJIMA, R. NINOMIYA and K. KUBOTA, *Corrosion Reviews* **16** (1998) 139.
10. "The ASM Metals Handbook," Vol. 9, edited by the ASM Handbook Committee (The Materials Research Information Society, USA, 1992) p. 425.
11. Z. SZKLARSKA-SMIALOWSKA, "Pitting Corrosion of Metals" (National Association of Corrosion Engineers, Houston, Texas, 1988) p. 399–402.
12. E. F. EMLEY, "Principles of Magnesium Technology" (Pergamon Press, Oxford, 1966) p. 214.
13. G. SONG, A. ATRENS, D. STJOHN, J. NAIRN and Y. LI, *Corrosion Science* **39** (1997) 855.
14. G. SONG, A. ATRENS, D. STJOHN, X. WU and J. NAIRN, *ibid.* **39** (1997) 1981.
15. G. SONG, A. ATRENS, X. WU and B. ZHANG, *ibid.* **40** (1998) 1769.
16. L. L. SHREIR, R. A. JARMAN and G. T. BURSTEIN, "Corrosion" (Butterworth–Heinemann Ltd., Oxford, 1994) p. 4–169.

Received 4 March
and accepted 15 July 1999